Revisiting giant photoelectron asymmetries in fenchone enantiomers

Laura Sommerlad,[1,*] Nikolay M. Novikovskiy,[2] Florian Trinter,[3] Dominik Stemer,[3] Owen Dennis McGinnis,[1] Andreas Pier,[1] Niklas Melzer,[1] Jan Kruse,[1] Max Kircher,[1] Leon Kaiser,[1] Theresa Wenzel,[1] Till Jahnke,[4] Reinhard Dörner,[1] Philipp V. Demekhin,[2] and Markus S. Schöffler[1,†]

[1]*Institut für Kernphysik, Goethe-Universität, Max-von-Laue-Straße 1, 60438 Frankfurt am Main, Germany*
[2]*Institut für Physik und CINSaT, Universität Kassel, Heinrich-Plett-Straße 40, 34132 Kassel, Germany*
[3]*Molecular Physics, Fritz-Haber-Institut der Max-Planck-Gesellschaft, Faradayweg 4–6, 14195 Berlin, Germany*
[4]*Max-Planck-Institut für Kernphysik, Saupfercheckweg 1, Heidelberg, Germany*

(Received 19 February 2026; accepted 6 May 2026; published 27 May 2026)

We report a joint experimental and theoretical study of core ionization of fenchone enantiomers at photon energies in the range 294.9–306.9 eV. Our experimental method enables the measurement of photoelectron momentum distributions with full 4π solid-angle coverage in the laboratory frame, yielding photon-energy-resolved dichroic and anisotropy parameters for photoelectrons emitted from C 1*s* (C=O and C–H_n) orbitals. Our experimental results are supported by *ab initio* electronic-structure calculations and agree fairly well with values available in the literature. Our findings demonstrate that core-level photoelectron circular dichroism is highly sensitive to both the localization of the emitting orbital and the treatment of background contributions, providing a solid basis for future studies of complex chiral molecules.

DOI: 10.1103/jw4j-gfd8

I. INTRODUCTION

Since its first theoretical description in 1976 [1] and experimental validation almost 25 years later [2], photoelectron circular dichroism (PECD) has emerged as a powerful tool for investigating the interaction of chiral molecules with light. A comprehensive overview of experimental and theoretical PECD studies conducted over the past two decades can be found in a very recent review article [3]. The PECD effect manifests as a light-helicity-dependent forward-backward asymmetry in the angular distribution of photoelectrons emitted from chiral molecules ionized by circularly polarized light. As PECD is governed by an electric-dipole transition [1], the measured asymmetries typically range on the order of a few percent, demonstrating the potential of PECD as a sensitive method for chiral recognition [4]—an aspect of critical importance in medical and biochemical applications.

So far, extensive experimental and theoretical investigations have explored PECD across different photon-energy regimes. PECD has been observed not only in single- and multiphoton ionization but also in strong-field ionization processes [5], emphasizing its fundamental role in chiral light-matter interactions. Although early studies targeted the ionization of outer molecular orbitals, sizable PECD has also been observed in the inner-shell ionization of chiral molecules [6]. From a physical perspective, in this case, the effect originates from diffraction of the emitted photoelectron wave by the chiral molecular potential, making it a final-state scattering phenomenon [3]. Recent studies of the inner-shell photoionization of trifluoromethyloxirane molecules have demonstrated that PECD depends substantially on both the orbital from which the electron is ejected [7] and the kinetic energy of the emitted photoelectron [8].

Previous experimental and theoretical studies have extensively investigated photoelectron circular dichroism in fenchone across different ionization regimes and intermediate-state dynamics, providing an important foundation for the present work [9–15]. In 2008, Ulrich *et al.* [16] reported exceptionally large PECD asymmetry signals—up to 20%—following C 1*s* ionization of fenchone molecules. This discovery established fenchone as a compelling target for further investigation. More recently, PECD studies have examined fenchone in the liquid phase [17], as well as in time-resolved valence-shell ionization experiments [18], reinforcing its role as a prototype system. In this study, we revisit the giant PECD asymmetry reported by Ulrich *et al.* [16] for two reasons. First, it allows for a direct verification and comparison of PECD measurements obtained using different experimental methodologies. Second, the molecular structure of fenchone provides a unique opportunity to examine how the location of the source of the photoelectron wave within the molecule influences the PECD effect.

As depicted in Fig. 1, fenchone consists of nine carbon–hydrogen (C–H_n) bonds and a single, well-localized carbon–oxygen (C=O) bond, separated by approximately 2.3 eV in their binding energies. Due to their similar chemical

*Contact author: Sommerlad@atom.uni-frankfurt.de
†Contact author: Schoeffler@atom.uni-frankfurt.de

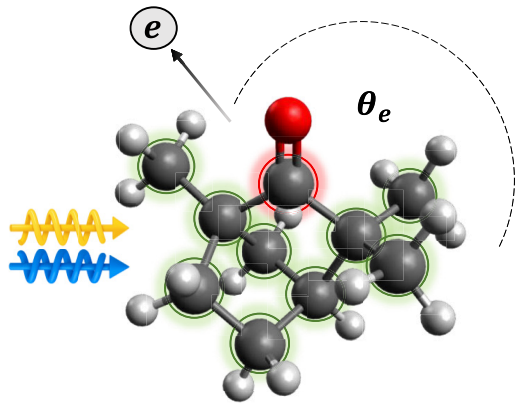

FIG. 1. Schematic illustration of the photoelectron measurement on (1*R*,4*S*)-fenchone. The red-highlighted carbon atom is double bonded to an oxygen atom, forming a carbonyl (C=O) group. The remaining green-highlighted carbon atoms are each bonded to n hydrogen atoms ($n = 0$–3). Photoelectrons emitted from the C 1*s* (C=O) orbital of the carbonyl group exhibit a kinetic energy approximately 2.3 eV lower than those emitted from the C 1*s* orbitals of the C–H_n bonded atoms. The emission angle θ_e between the photoelectron momentum vector and the light propagation direction is measured for both positive and negative light helicities. See Sec. II for experimental details.

environments, the binding energies of C 1*s* (C–H_n) photoelectrons are very close, and these photoelectrons manifest as a single broad peak in X-ray photoelectron spectroscopy [18]. Previous studies suggested that the collective contribution of C 1*s* (C–H_n) photoelectrons results in a net PECD effect of almost zero [6]. In Ref. [16], it was shown that, for a specific energy, a net PECD can be observed, meaning that the previous statement is not generally valid. Recent theoretical calculations support this assumption by predicting that, at certain photoelectron energies, the PECD of C 1*s* (C–H_n) photoelectrons may even be comparable to that of C 1*s* (C=O) photoelectrons [18]. This finding underscores the need for further experimental verification and deeper theoretical insights into the role of electron localization in PECD.

II. EXPERIMENT

The experiment was conducted using a cold target recoil ion momentum spectroscopy (COLTRIMS) reaction microscope [19], in which a molecular beam of fenchone molecules was intersected with a photon beam provided by beamline P04 [20] at the PETRA III synchrotron (DESY, Hamburg, Germany). The synchrotron was operated in 40-bunch mode (5.2 MHz), corresponding to a bunch spacing of 192 ns. This timing structure allows unambiguous electron time-of-flight measurements, with the bunch-marker signal providing the start time. Commercially available samples of the (1*R*,4*S*)-(−)-fenchone (Sigma-Aldrich, W507709, ⩾98%) and (1*S*,4*R*)-(+)-fenchone (Sigma-Aldrich, 46120, ⩾98%) enantiomers were used without further purification. The stainless-steel sample container, together with the associated gas lines and the 200 μm nozzle, was maintained at a controlled temperature between 70 and 85 °C to ensure stable vaporization. The molecular beam was generated by expanding fenchone vapor through the 200 μm nozzle into vacuum. While this expansion does not correspond to a fully developed seeded supersonic jet, differential pumping combined with two skimming stages (each 300 μm in diameter) produces a well-defined, directed molecular beam under weakly collisional conditions. Circularly polarized photons with energies ranging from 294.9 to 306.9 eV were employed. For each enantiomer and photon energy, left- and right-circularly polarized measurements were recorded for 1 h each. A single left-right cycle was sufficient to generate each data point shown in Figs. 4 and 5, with a total acquisition time of approximately 30 h. The (1*S*,4*R*)-enantiomer was studied at photon energies from 294.9 to 300.9 eV in steps of 1 eV, while the (1*R*,4*S*)-enantiomer was measured at 298.9, 300.9, 302.9, 304.9, and 306.9 eV. The photon energy was calibrated using argon by measuring the kinetic energies of the Ar $2p_{1/2}$ and Ar $2p_{3/2}$ photoelectrons and shifting the energy scale to match the reference values reported in Ref. [21].

The charged fragments generated in the interaction region were guided toward two time- and position-sensitive detectors [22] by a combination of electric and magnetic fields. The three-dimensional momentum vectors of the electrons were reconstructed based on their times of flight and impact positions. This momentum information provided access to the photoelectron emission angle θ_e relative to the propagation direction of the incident light. The COLTRIMS spectrometer field configuration was optimized to ensure a 4π detection efficiency for photoelectrons with kinetic energies up to 17 eV. Specifically, the spectrometer consisted of a 42.1 cm electron arm (14.3 cm acceleration and 27.8 cm drift) and a 13.3 cm ion arm. The extraction field in the target region was 5 V/cm and the magnetic field was 4.7 G. For a meaningful comparison with existing electron-spectroscopy results, our study focuses exclusively on the analysis of photoelectron properties, integrating over all molecular fragmentation channels and fragment-ion emission angles.

To characterize the employed samples, we performed absorption-based electron circular dichroism (CD) measurements using a commercial Chirascan V100 CD spectrophotometer (Applied Photophysics). Dilute solutions of fenchone in ethanol (62.3 mM) were measured in a quartz cuvette with a 1 mm path length. Background subtraction was performed using a pure ethanol reference measurement. For both enantiomers of fenchone, we measured the circular dichroism in a wavelength range of 200–400 nm. The step size for each measurement was 1 nm. The data are displayed in Fig. 2 in units of molar ellipticity.

A. Dichroic and asymmetry parameter

We analyzed the angle-resolved electron spectra recorded for randomly oriented fenchone enantiomers at the above-mentioned photon energies for the two photon helicities ($I_\pm$). To account for possible variations in photon flux and sample pressure, the measured spectra were normalized to their respective integrals. To describe the normalized photoelectron angular distributions, we utilized the parametrization within the dipole approximation regime [23]

$$\bar{I}_\pm(\theta_e) = \frac{1}{I_{\pm,int}}\left(1 \pm b_1 P_1(\cos\theta_e) - \frac{1}{2} b_2 P_2(\cos\theta_e)\right), \quad (1)$$

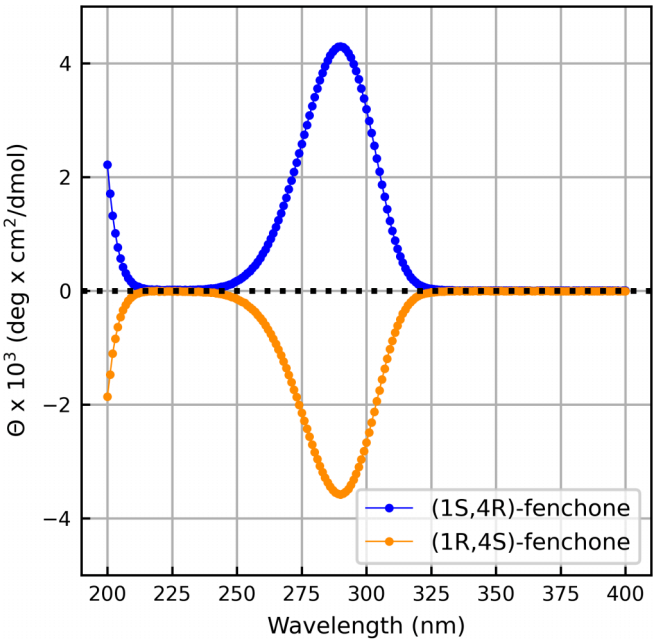

FIG. 2. Circular dichroism spectra of the (1*S*,4*R*)- and (1*R*,4*S*)-fenchone enantiomers. The difference in signal intensity between the enantiomers suggests a disparity in enantiomeric purity, as further discussed in Sec. IV.

with the dichroic parameter b_1, the anisotropy parameter b_2, and the first two Legendre polynomials P_1 and P_2. The value of b_2 was derived from the sum of the angular distributions obtained using positive and negative helicities, while b_1 was extracted from the difference between these distributions. This approach yields the standard expression of the PECD signal:

$$\mathrm{PECD} = \frac{\bar{I}_+(\theta_e) - \bar{I}_-(\theta_e)}{\bar{I}_+(\theta_e) + \bar{I}_-(\theta_e)} = \frac{b_1 P_1(\cos\theta_e)}{1 - \frac{1}{2} b_2 P_2(\cos\theta_e)}. \quad (2)$$

Direct application of Eq. (2) as a fitting function to extract both b_1 and b_2 simultaneously is reliable only if b_1 does not approach zero. To ensure a stable fitting procedure, the denominator of Eq. (2), $\bar{I}_+(\theta_e) + \bar{I}_-(\theta_e)$, is first used independently to extract the anisotropy parameter b_2. This value is held fixed in a second fitting step, in which the full equation is used to determine the dichroic parameter b_1.

B. Background subtraction

In addition, it is essential to take into account the background signal underlying the photoelectron peaks. This background contribution is particularly significant for the C 1*s* (C=O) photoelectron peak, where it accounts for approximately 40%–50% of the total electron signal. Consequently, three different types of background contributions must be considered. The first originates from the ionization of residual gas and warm fenchone molecules in the reaction chamber and represents approximately 3% of the total background signal. The second background contribution arises from false electron signals, which may be produced, for example, by electron scattering induced by the halo of the photon beam. This type of background is estimated from measurements performed without the target gas and represents approximately 20% of

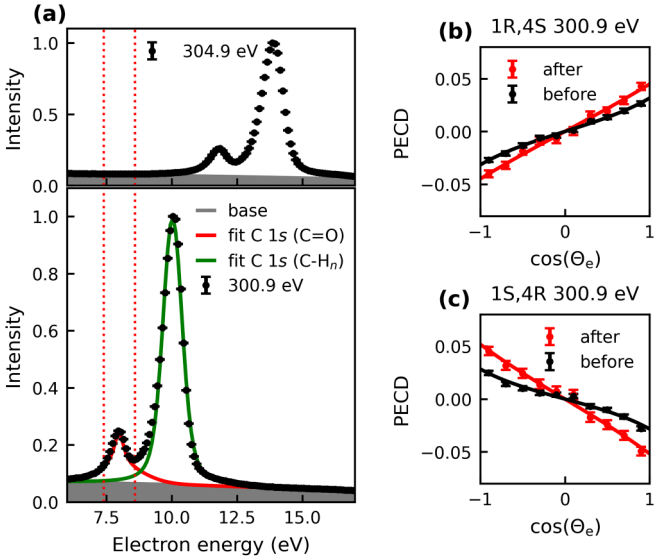

FIG. 3. Exemplary background subtraction procedure for C 1*s* (C=O) ionization at a photon energy of 300.9 eV (see text for details). (a) Electron energy distributions of (1*R*,4*S*)-fenchone recorded at $h\nu = 304.9$ eV (upper panel) and $h\nu = 300.9$ eV (lower panel). The red and green curves represent the fit results for the C 1*s* (C=O) and C 1*s* (C–H_n) photoelectron peaks, respectively. The dashed line indicates the energy gate used in the analysis. The dominant background component beneath the photoelectron peaks, shown in gray, is estimated from the 304.9 eV data. (b) PECD values [see Eq. (2)] for (1*R*,4*S*)-fenchone. Black data points represent the measured values with statistical error bars before background subtraction. Red data points show the corrected values, with uncertainties calculated according to Eq. (6). (c) Same as panel (b), but for (1*S*,4*R*)-fenchone.

the background signal underlying the C 1*s* (C=O) peak. Such background could be reduced by employing electron-ion coincidence detection. However, in our experiment, the ions were not detected with full 4π solid-angle coverage. Additionally, the low electric field required for sufficient electron energy resolution impairs ion mass identification due to significant overlap in the time of flight. Applying a coincidence gate on the ions would therefore introduce a bias by selecting specific molecular orientations. To preserve a random distribution of molecular orientations in the analysis, ion-electron coincidences were not employed. The third and dominant type of background is intrinsic in nature, primarily originating from physical processes such as multiple Auger decays/Auger cascades and satellite transitions. These contributions distort the measured dichroic and anisotropy parameters, necessitating a rigorous background subtraction procedure. In our approach, we assume that the background present in the electron energy distribution remains nearly constant across comparable photon energies. For instance, to subtract the background from the spectrum recorded at $h\nu = 300.9$ eV, we use the corresponding part of the spectrum measured at $h\nu = 304.9$ eV [see Fig. 3(a) for clarification].

The background subtraction is carried out in multiple steps. First, we estimate the background beneath the C=O and C–H_n photoelectron peaks. The dominant component, highlighted in gray in Fig. 3(a), is attributed to the aforementioned physical processes. This baseline is fitted using asymmetric

least-squares smoothing [24]. From the integrated baseline fit N_b, the fractional background contribution beneath the photoelectron peak is given by $f_b = N_b/N_{\text{meas}}$, where N_{meas} denotes the total number of counts within the energy gate defining the measured photoelectron peak. For the example shown in Fig. 3(a), the baseline contributes $f_b = 34\%$ to the photoelectron signal. Because the C=O and C–H_n peaks partially overlap, each contributes to the apparent background of the other. A pseudo-Voigt function is used to fit the C=O peak, while a Voigt function is applied to the C–H_n peak. These fits enable us to quantify the background contribution arising from the neighboring peak, expressed as $f_{\text{np}} = N_{\text{np}}/N_{\text{meas}}$, which amounts to $f_{\text{np}} = 8\%$ in Fig. 3(a). We then subtract this background from the measured angular distribution $I_{\text{meas}}(\theta_e)$. We distinguish between a baseline component, $I_b(\theta_e)$, and a neighboring-peak contribution, $I_{\text{np}}(\theta_e)$. The distribution $I_b(\theta_e)$ is taken from a dataset recorded at a different but comparable photon energy, whereas $I_{\text{np}}(\theta_e)$ is extracted from data acquired at the same photon energy. Both components are scaled by their relative weights, given by

$$n_b = f_b \times \frac{N_{\text{meas}}}{I_{b,\text{int}}} = \frac{N_b}{I_{b,\text{int}}} \tag{3}$$

and

$$n_{\text{np}} = f_{\text{np}} \times \frac{N_{\text{meas}}}{I_{\text{np,int}}} = \frac{N_{\text{np}}}{I_{\text{np,int}}}, \tag{4}$$

where $I_{b,\text{int}}$ and $I_{\text{np,int}}$ denote the angle-integrated intensities of $I_b(\theta_e)$ and $I_{\text{np}}(\theta_e)$ used for background subtraction. The scaled background distributions are subtracted from the measured angular distribution, and the result is normalized by the angle-integrated corrected intensity to obtain the final background-corrected signal:

$$\bar{I}_{\text{corr}}(\theta_e) = \frac{I_{\text{meas}}(\theta_e) - n_b I_b(\theta_e) - n_{\text{np}} I_{\text{np}}(\theta_e)}{I_{\text{corr,int}}}. \tag{5}$$

The associated uncertainty is approximated as

$$\Delta\bar{I}_{\text{corr}}(\theta_e) \approx \frac{\sqrt{\begin{array}{l}(\Delta I_{\text{meas}})^2 + (n_b \Delta I_b)^2 + (n_{\text{np}} \Delta I_{\text{np}})^2 \\ + (I_b \Delta n_b)^2 + (I_{\text{np}} \Delta n_{\text{np}})^2\end{array}}}{I_{\text{corr,int}}}, \tag{6}$$

where ΔI_{meas}, ΔI_b, and ΔI_{np} denote the respective statistical uncertainties, and Δn_b, Δn_{np} arise from the fitting procedure. As the background is forward-backward symmetric, the main effect of the background correction is an increase in the dichroic parameter b_1. For the case shown in Fig. 3, we obtain $b_1 = 0.032$ ($= 0.051$) before (after) the background correction for the (1*R*,4*S*)-enantiomer [black and red curves in Fig. 3(b)], while for the (1*S*,4*R*)-enantiomer in Fig. 3(c), it is $b_1 = -0.024$ ($= -0.049$), respectively.

III. THEORETICAL CALCULATIONS

We performed our calculations only for C 1*s* (C=O) photoionization of fenchone using the stationary single-center method [25–27], in a manner similar to our previous study of the O 1*s* photoionization of this molecule [28]. The calculations were carried out in the relaxed-core Hartree-Fock (RCHF) approximation at the equilibrium internuclear geometry of the ground electronic state of the neutral molecule. Partial photoelectron continuum waves were obtained in the ionic potential of a singly charged molecule, which includes a monopole relaxation of all occupied orbitals caused by the created core vacancy. This effect was simulated in the equivalent-core approximation with a fractional nuclear charge for the core-ionized atom [29,30]. For this purpose, all occupied orbitals of the ion were generated in a molecule containing all 84 electrons, with the nuclear charge of the carbon atom in the C=O group set to 6.5 (as optimized in Refs. [29,30]), thereby modeling relaxation on a half of the created core vacancy. These occupied molecular orbitals were generated using the PC GAMESS (US) [31] quantum chemistry package with a triple-zeta valence basis set [32] augmented by two *p*-type and one *d*-type polarization functions. The orbitals were further represented by single-center expansions with angular momentum quantum numbers ℓ, $|m| \leqslant 99$ and used to generate the ionic potential of the C 1*s* (C=O) core-ionized molecule for the photoelectron waves with ℓ, $|m| \leqslant 29$. The dichroic and anisotropy parameters were calculated via the explicit equations reported in Refs. [33,34].

IV. RESULTS AND DISCUSSION

In our experiment, we measured the full momentum distribution of the photoelectrons, covering all emission directions in the laboratory frame. This provides access to the dichroic parameter b_1 and the anisotropy parameter b_2 as functions of both the electron and photon energies. The absolute electron kinetic energies were determined from the calibrated photon energies and the binding energies reported in Ref. [16], namely, $IP_{\text{C 1}s\,(\text{C–H}_n)} = 290.3$ eV and $IP_{\text{C 1}s\,(\text{C=O})} = 292.6$ eV. The dichroic parameter characterizes the strength of the PECD signal and, ideally, should have identical absolute values for both enantiomers, albeit with opposite signs. To verify this, we measured both enantiomers at two photon energies, 298.9 and 300.9 eV, as an internal consistency check. A meaningful comparison also requires assessing the enantiomeric purity of the samples, as this factor influences the observed PECD magnitude. Variations in the enantiomeric purity of commercially available samples of (1*R*,4*S*)-fenchone have been reported in previous studies [35–37]. Consistent with this, the circular-dichroism measurement shown in Fig. 2 reveals a notable difference in signal intensity between the two enantiomers, indicating a significant variation in enantiomeric purity. Specifically, the maximum CD signal for (1*S*,4*R*)-fenchone is approximately 1.2 times that of (1*R*,4*S*)-fenchone. This disparity results in different absolute values of the PECD signal measured for the two enantiomers. To correct for this difference in enantiomeric purity, the measured values of b_1 for (1*R*,4*S*)-fenchone were scaled accordingly.

Figure 4 shows the measured values of the dichroic parameter b_1 and the anisotropy parameter b_2 for C 1*s* (C–H_n) photoelectrons, spanning kinetic energies from about 4 to 15 eV. To illustrate the influence of the underlying background in the measured data, we included error bands in the plot, representing the difference between the background-subtracted data and the raw data without background subtraction. The large ionization cross section of the C 1*s* (C–H_n) peak

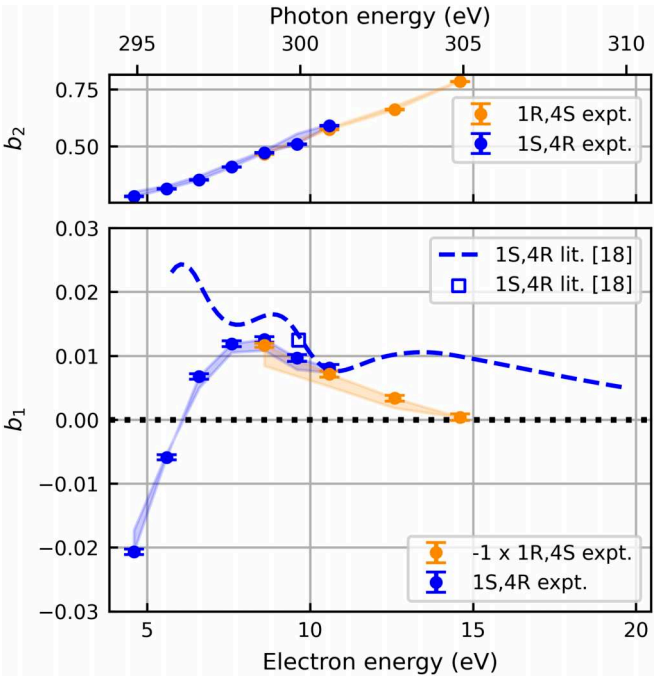

FIG. 4. Experimental and theoretical results of C 1s (C–H$_n$) ionization of the (1S,4R)-fenchone (blue) and (1R,4S)-fenchone (orange) enantiomers. The upper and lower panels display the photon- and electron-energy-resolved anisotropy parameter b_2 and the dichroic parameter b_1, respectively. Solid symbols with error bars represent our experimental data points, corrected for the measured difference in enantiopurity (see text). The blue and orange error bands represent experimental values obtained without background subtraction. The blue dashed curve (theory) and the open symbols (experiment) are taken from Ref. [18].

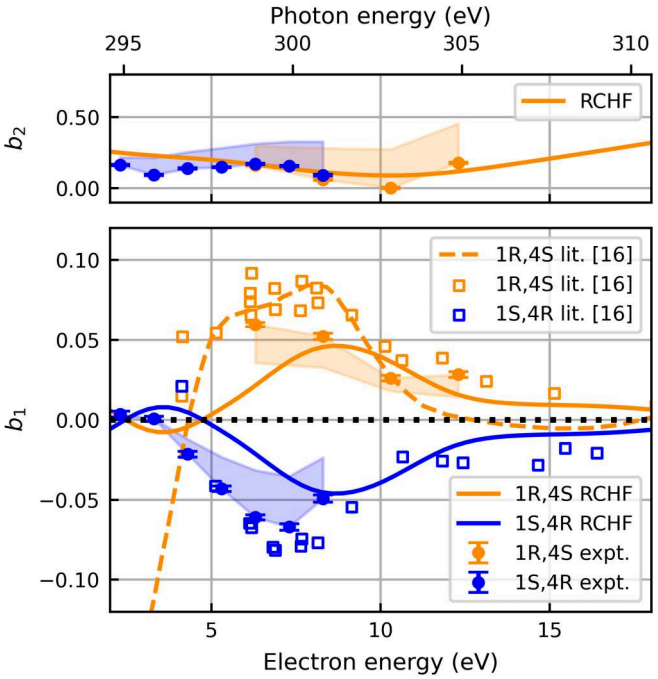

FIG. 5. Experimental and theoretical results for the (1S,4R)-fenchone (blue) and (1R,4S)-fenchone (orange) enantiomers following C 1s (C=O) ionization. The upper and lower panels depict the photon- and electron-energy-resolved anisotropy parameter b_2 and the dichroic parameter b_1, respectively. Solid symbols with error bars represent our experimental data points, corrected for the measured difference in enantiopurity (see text). The blue and orange error bands represent experimental values obtained without background subtraction. Solid lines correspond to the present RCHF calculations. Open symbols and the dashed curve represent, respectively, experimental and theoretical data from Ref. [16].

naturally results in a low background contribution, as reflected in the narrow error bands. The extracted values of the dichroic parameter lie within a few percent. The anisotropy parameter increases with electron kinetic energy and is expected to saturate at $b_2 = 2$, representing ionization of an atomic s state. In molecules, this value is reduced by scattering of the electron on its way out of the molecular scaffold; neglecting shape resonances, the scattering decreases with increasing electron energy.

It is not possible to separate the individual contributions of the nine C–H$_n$ bound carbon atoms in the measured spectra. Nevertheless, the observed asymmetry can be interpreted as a net forward-backward asymmetry arising from the superposition of the photoelectron signals from the individual C 1s contributions, adding up incoherently. In previous studies (Refs. [16,18]), it was suggested that all overlapping C 1s (C–H$_n$) contributions approximately cancel out, such that averaging over them would result in a net PECD effect close to zero. In contrast, the asymmetry values observed in our measurements, though small, do not cancel out. Time-dependent *ab initio* calculations reported in Ref. [18] predict the energy-resolved dichroic parameter for the averaged contribution of individual C 1s (C–H$_n$) photoelectrons, which we plot together with one experimental data point at a photon energy of 300 eV (dashed blue curve and open blue symbol in Fig. 4). Our experimental data show good agreement with these theoretical predictions in the kinetic-energy range of 7–11 eV. However, for lower and higher kinetic energies, our experimentally obtained values do not support the theoretical predictions of Ref. [18].

In contrast to the relatively sparse data available for C 1s (C–H$_n$) photoelectrons, extensive experimental and theoretical results have been reported in the literature for C 1s (C=O) photoelectrons. Our experimental findings for both the dichroic b_1 and the anisotropy b_2 parameters, together with the present RCHF calculations, are compared in Fig. 5 with the available experimental and theoretical data from Ref. [16]. Overall, our experimental results are in good agreement with the present theoretical results for b_1 and b_2, successfully reproducing the general trend of the energy-resolved dichroic parameter reported in the literature. The data points measured at 298.9 and 300.9 eV for both enantiomers show good agreement, differing only in sign.

We do not observe the sign change in b_1 at a kinetic energy of approximately 3 eV, as suggested by the computed and measured data from Ref. [16] and by our theory. In addition, the present experiment and theory do not support the sign change in b_1 at a kinetic energy of approximately 12 eV, as proposed by the calculations of Ref. [16]. Moreover, the absolute values of b_1 obtained in our measurements appear to be slightly shifted in energy and are somewhat lower than

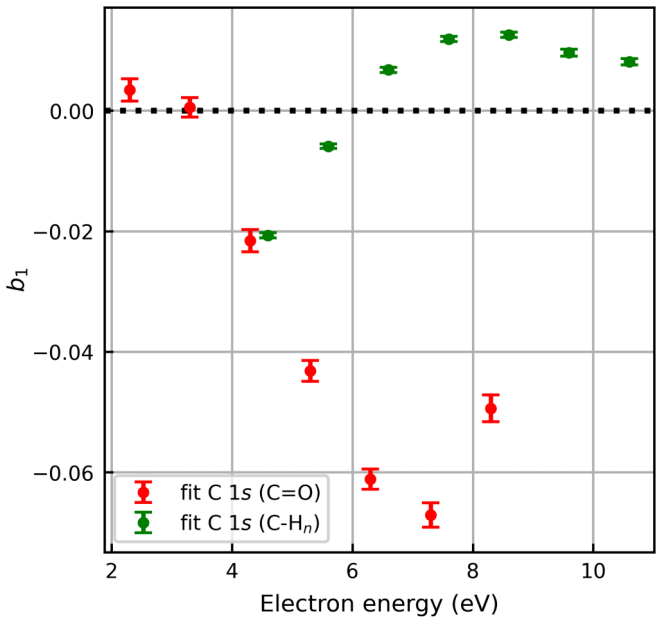

FIG. 6. Comparison of the measured energy-resolved dichroic parameters for C 1s (C=O) (red symbols) and C 1s (C–H$_n$) (green symbols) photoelectrons in (1S,4R)-fenchone.

those reported in Ref. [16]. The relatively large error bands indicate a significant background contribution underlying the C 1s (C=O) peak, which must be considered when analyzing and interpreting the absolute values of the dichroic parameter. Therefore, employing different approaches in the treatment or estimation of the underlying background may explain the observed differences between our results and the previously reported experimental values of b_1.

In the case of C 1s (C=O) ionization, the emitted photoelectrons originate from a well-defined distance relative to the chiral center at the instant of photoionization. In contrast, for C 1s (C–H$_n$) ionization, this distance spans a distribution of values. The C 1s (C=O) photoelectrons may therefore be considered to come from a spatially localized source, in contrast to the delocalized nature of C 1s (C–H$_n$) photoelectron sources. A comparison of the energy-resolved PECD signals for these two cases enables an assessment of how, for a fixed photon energy, both the kinetic energy and the emission site of the electron influence the PECD. A direct comparison between the energy-resolved dichroic parameters for C 1s (C=O) and C 1s (C–H$_n$) photoelectrons in (1S,4R)-fenchone is shown in Fig. 6. As shown, the magnitude of b_1 for the C–H$_n$ sites is consistently lower than that for the C=O site, with the largest absolute difference occurring at a kinetic energy of approximately 8 eV. At this energy, the dichroic parameter for C=O is about seven times larger than that for C–H$_n$. In contrast, at a kinetic energy of 5 eV, the measured asymmetries are very similar. The overall trend of the dichroic parameter not only differs substantially between C=O and C–H$_n$, but also exhibits an opposite sign above approximately 7 eV. These observations indicate that the spatial origin of the photoelectron within the molecule has a stronger influence on PECD than the photoelectron kinetic energy alone. This sensitivity of the photoelectron wave indicates that inner-shell PECD is caused by scattering mainly at small distances inside the molecule and is not dominated by the long-range part of the potential.

V. CONCLUSION

We have measured the energy-resolved dichroic (b_1) and anisotropy (b_2) parameters of the C 1s photoelectrons for spatially localized (C=O bound) and delocalized (C–H$_n$ bound) emitters in fenchone enantiomers. Our experimental results are supported by relaxed-core Hartree-Fock calculations. Furthermore, we have demonstrated the critical importance of a proper treatment of the background underlying the photoelectron peaks—an issue particularly relevant for core-level ionization in larger molecular systems. To mitigate background interference in core-hole ionization measurements, we propose focusing on momentum-conserving two-body breakup events, in which the only emitted particles are a photoelectron and a high-energy Auger electron. This approach would, in principle, eliminate the dominant systematic background of low-energy electrons from secondary decay routes and could represent a promising strategy for future PECD measurements using a reaction microscope. Using this method, PECD in fenchone enantiomers could also be investigated as a function of a single molecular breakup axis, similar to the approach of Refs. [38,39]. Furthermore, our findings reveal a nonzero net forward-backward asymmetry in the emission from delocalized C–H$_n$ emitters. However, a complete interpretation of the PECD signal—specifically, the decomposition into contributions from individual C 1s (C–H$_n$) photoelectrons—remains experimentally inaccessible. Overall, our work suggests that PECD depends more strongly on the spatial origin of the emitted photoelectron than on its kinetic energy. This highlights the need for further investigation into the microscopic origins of PECD in complex chiral molecules.

ACKNOWLEDGMENTS

We acknowledge DESY (Hamburg, Germany), a member of the Helmholtz Association HGF, for the provision of experimental facilities. Parts of this research were carried out at PETRA III. Data were collected using beamline P04 operated by DESY Photon Science. We would like to thank the P04 team for assistance during the experiments. Beamtime was allocated for Proposal No. I-20221169. This work was funded by the Deutsche Forschungsgemeinschaft (DFG, German Research Foundation)—Project No. 328961117—SFB 1319 ELCH (Extreme light for sensing and driving molecular chirality). F.T. acknowledges funding by the DFG—Project No. 509471550, Emmy Noether Programme. D.S. acknowledges funding from the European Research Council (ERC) under the European Union's Horizon 2020 research and innovation program under Grant Agreement No. GAP 883759–AQUACHIRAL.

DATA AVAILABILITY

The data that support the findings of this article are not publicly available upon publication because it is not

technically feasible and/or the cost of preparing, depositing, and hosting the data would be prohibitive within the terms of this research project. The data are available from the authors upon reasonable request.

[1] B. Ritchie, Theory of the angular distribution of photoelectrons ejected from optically active molecules and molecular negative ions, Phys. Rev. A **13**, 1411 (1976).

[2] N. Böwering, T. Lischke, B. Schmidtke, N. Müller, T. Khalil, and U. Heinzmann, Asymmetry in photoelectron emission from chiral molecules induced by circularly polarized light, Phys. Rev. Lett. **86**, 1187 (2001).

[3] C. Sparling and D. Townsend, Two decades of imaging photoelectron circular dichroism: From first principles to future perspectives, Phys. Chem. Chem. Phys. **27**, 2888 (2025).

[4] I. Powis, Photoelectron circular dichroism: Chiral asymmetry in the angular distribution of electrons emitted by (+)-*S*-carvone, Chirality **20**, 961 (2008).

[5] S. Beaulieu, A. Ferré, R. Géneaux, R. Canonge, D. Descamps, B. Fabre, N. Fedorov, F. Légaré, S. Petit, T. Ruchon, V. Blanchet, Y. Mairesse, and B. Pons, Universality of photoelectron circular dichroism in the photoionization of chiral molecules, New J. Phys. **18**, 102002 (2016).

[6] U. Hergenhahn, E. E. Rennie, O. Kugeler, S. Marburger, T. Lischke, I. Powis, and G. Garcia, Photoelectron circular dichroism in core level ionization of randomly oriented pure enantiomers of the chiral molecule camphor, J. Chem. Phys. **120**, 4553 (2004).

[7] K. Fehre, F. Trinter, N. M. Novikovskiy, S. Grundmann, D. Tsitsonis, S. Eckart, L. Bauer, M. Hilzinger, T. Jahnke, R. Dörner, P. V. Demekhin, and M. S. Schöffler, Influence of the emission site on the photoelectron circular dichroism in trifluoromethyloxirane, Phys. Chem. Chem. Phys. **24**, 13597 (2022).

[8] G. Nalin, K. Fehre, F. Trinter, N. M. Novikovskiy, N. Anders, D. Trabert, S. Grundmann, M. Kircher, A. Khan, R. Tomar, *et al.*, Photoelectron circular dichroism of O 1*s*-photoelectrons of uniaxially oriented trifluoromethyloxirane: Energy dependence and sensitivity to molecular configuration, Phys. Chem. Chem. Phys. **23**, 17248 (2021).

[9] C. Lux, M. Wollenhaupt, T. Bolze, Q. Liang, J. Köhler, C. Sarpe, and T. Baumert, Circular dichroism in the photoelectron angular distributions of camphor and fenchone from multiphoton ionization with femtosecond laser pulses, Angew. Chem. Int. Ed. **51**, 5001 (2012).

[10] A. Kastner, T. Ring, B. C. Krüger, G. B. Park, T. Schäfer, A. Senftleben, and T. Baumert, Intermediate state dependence of the photoelectron circular dichroism of fenchone observed via femtosecond resonance-enhanced multi-photon ionization, J. Chem. Phys. **147**, 013926 (2017).

[11] A. D. Müller, A. N. Artemyev, and P. V. Demekhin, Photoelectron circular dichroism in the multiphoton ionization by short laser pulses. II. Three- and four-photon ionization of fenchone and camphor, J. Chem. Phys. **148**, 214307 (2018).

[12] A. D. Müller, E. Kutscher, A. N. Artemyev, and P. V. Demekhin, Photoelectron circular dichroism in the multiphoton ionization by short laser pulses. III. Photoionization of fenchone in different regimes, J. Chem. Phys. **152**, 044302 (2020).

[13] V. Blanchet, D. Descamps, S. Petit, Y. Mairesse, B. Ponsa, and B. Fabre, Ultrafast relaxation investigated by photoelectron circular dichroism: An isomeric comparison of camphor and fenchone, Phys. Chem. Chem. Phys. **23**, 25612 (2021).

[14] D. P. Singh, J. O. F. Thompson, K. L. Reid, and I. Powis, Influence of vibrational excitation and nuclear dynamics in multiphoton photoelectron circular dichroism of fenchone, J. Phys. Chem. Lett. **12**, 11438 (2021).

[15] E. Kutscher, A. N. Artemyev, and P. V. Demekhin, Photoelectron circular dichroism in fenchone by short coherent broadband laser pulses, Phys. Rev. A **107**, 013107 (2023).

[16] V. Ulrich, S. Barth, S. Joshi, U. Hergenhahn, E. Mikajlo, C. J. Harding, and I. Powis, Giant chiral asymmetry in the C 1*s* core level photoemission from randomly oriented fenchone enantiomers, J. Phys. Chem. A **112**, 3544 (2008).

[17] M. N. Pohl, S. Malerz, F. Trinter, C. Lee, C. Kolbeck, I. Wilkinson, S. Thürmer, D. M. Neumark, L. Nahon, I. Powis, G. Meijer, B. Winter, and U. Hergenhahn, Photoelectron circular dichroism in angle-resolved photoemission from liquid fenchone, Phys. Chem. Chem. Phys. **24**, 8081 (2022).

[18] D. Facciala, M. Devetta, S. Beauvarlet, N. Besley, F. Calegari, C. Callegari, D. Catone, E. Cinquanta, A. G. Ciriolo, L. Colaizzi, *et al.*, Time-resolved chiral X-ray photoelectron spectroscopy with transiently enhanced atomic site selectivity: A free-electron laser investigation of electronically excited fenchone enantiomers, Phys. Rev. X **13**, 011044 (2023).

[19] J. Ullrich, R. Moshammer, A. Dorn, R. Dörner, L. P. H. Schmidt, and H. Schmidt-Böcking, Recoil-ion and electron momentum spectroscopy: Reaction-microscopes, Rep. Prog. Phys. **66**, 1463 (2003).

[20] J. Viefhaus, F. Scholz, S. Deinert, L. Glaser, M. Ilchen, J. Seltmann, P. Walter, and F. Siewert, The variable polarization XUV beamline P04 at PETRA III: Optics, mechanics and their performance, Nucl. Instrum. Methods Phys. Res. Sect. A **710**, 151 (2013).

[21] G. C. King, M. Tronct, F. H. Read, and R. C. Bradford, An investigation of the structure near the $L_{2,3}$ edges of argon, the $M_{4,5}$ edges of krypton and the $N_{4,5}$ edges of xenon, using electron impact with high resolution, J. Phys. B: Atom. Mol. Phys. **10**, 2479 (1977).

[22] O. Jagutzki, A. Cerezo, A. Czasch, R. Dörner, M. Hattaß, M. Huang, V. Mergel, U. Spillmann, K. Ullmann-Pfleger, T. Weber, H. Schmidt-Böcking, and G. D. W. Smith, Multiple hit readout of a microchannel plate detector with a three-layer delay-line anode, IEEE Trans. Nucl. Sci. **49**, 2477 (2002).

[23] L. Nahon, G. A. Garcia, C. J. Harding, E. Mikajlo, and I. Powis, Determination of chiral asymmetries in the valence photoionization of camphor enantiomers by photoelectron imaging using tunable circularly polarized light, J. Chem. Phys. **125**, 114309 (2006).

[24] P. H. C. Eilers and H. F. M. Boelens, Baseline correction with asymmetric least squares smoothing, Leiden University Medical Centre Report, 2005.

[25] P. V. Demekhin, A. Ehresmann, and V. L. Sukhorukov, Single center method: A computational tool for ionization and

electronic excitation studies of molecules, J. Chem. Phys. **134**, 024113 (2011).

[26] S. A. Galitskiy, A. N. Artemyev, K. Jänkälä, B. M. Lagutin, and P. V. Demekhin, Hartree-Fock calculation of the differential photoionization cross sections of small Li clusters, J. Chem. Phys. **142**, 034306 (2015).

[27] N. M. Novikovskiy, A. N. Artemyev, D. V. Rezvan, B. M. Lagutin, and P. V. Demekhin, Multichannel single center method, J. Phys. B: At. Mol. Opt. Phys. **55**, 175001 (2022).

[28] J. Leroux, D. Stemer, B. Credidio, F. Dudda, E. Heikura, A. Jose, A. Judt, C. Küstner-Wetekam, M. Zander, N. M. Novikovskiy, T. Otto, P. Patil, G. Petersen, S. Savio, N. Velasquez, N. Wieland, L. Wülfing, P. V. Demekhin, F. Trinter, and M. Ilchen, Oxygen-specific photoelectron circular dichroism in gas-phase fenchone, Phys. Rev. Res. **8**, 013340 (2026).

[29] N. A. Cherepkov, S. K. Semenov, A. V. Golovin, J. Adachi, and A. Yagishita, O K-shell photoemission of the CO molecule: Comparison between theory and experiment, J. Phys. B: At. Mol. Opt. Phys. **37**, 4803 (2004).

[30] S. K. Semenov, N. A. Cherepkov, T. Jahnke, and R. Dörner, Theoretical study of vibrationally resolved photoionization for the C K-shell of the CO molecule, J. Phys. B: At. Mol. Opt. Phys. **37**, 1331 (2004).

[31] M. W. Schmidt, K. K. Baldridge, J. A. Boatz, S. T. Elbert, M. S. Gordon, J. H. Jensen, S. Koseki, N. Matsunaga, K. A. Nguyen, S. Su, T. L. Windus, M. Dupuis, and J. A. Montgomery Jr., General atomic and molecular electronic structure system, J. Comput. Chem. **14**, 1347 (1993).

[32] T. H. Dunning, Jr., Gaussian basis functions for use in molecular calculations. III. Contraction of (10*s*6*p*) atomic basis sets for the first-row atoms, J. Chem. Phys. **55**, 716 (1971).

[33] A. Knie, M. Ilchen, P. Schmidt, P. Reiß, C. Ozga, B. Kambs, A. Hans, N. Müglich, S. A. Galitskiy, L. Glaser, P. Walter, J. Viefhaus, A. Ehresmann, and P. V. Demekhin, Angle-resolved study of resonant Auger decay and fluorescence emission processes after core excitations of the terminal and central nitrogen atoms in N_2O, Phys. Rev. A **90**, 013416 (2014).

[34] M. Ilchen, G. Hartmann, P. Rupprecht, A. N. Artemyev, R. N. Coffee, Z. Li, H. Ohldag, H. Ogasawara, T. Osipov, D. Ray, P. Schmidt, T. J. A. Wolf, A. Ehresmann, S. Moeller, A. Knie, and P. V. Demekhin, Emitter-site-selective photoelectron circular dichroism of trifluoromethyloxirane, Phys. Rev. A **95**, 053423 (2017).

[35] C. Lux, M. Wollenhaupt, C. Sarpe, and T. Baumert, Photoelectron circular dichroism of bicyclic ketones from multiphoton ionization with femtosecond laser pulses, ChemPhysChem **16**, 115 (2015).

[36] C. Lux, A. Senftleben, C. Sarpe, M. Wollenhaupt, and T. Baumert, Photoelectron circular dichroism observed in the above-threshold ionization signal from chiral molecules with femtosecond laser pulses, J. Phys. B: At. Mol. Opt. Phys. **49**, 02LT01 (2016).

[37] L. Nahon, L. Nag, G. A. Garcia, I. Myrgorodska, U. Meierhenrich, S. Beaulieu, V. Wanie, V. Blanchet, R. Géneaux, and I. Powis, Determination of accurate electron chiral asymmetries in fenchone and camphor in the VUV range: Sensitivity to isomerism and enantiomeric purity, Phys. Chem. Chem. Phys. **18**, 12696 (2016).

[38] M. Tia, M. Pitzer, G. Kastirke, J. Gatzke, H.-K. Kim, F. Trinter, J. Rist, A. Hartung, D. Trabert, J. Siebert, *et al.*, Observation of enhanced chiral asymmetries in the inner-shell photoionization of uniaxially oriented methyloxirane enantiomers, J. Phys. Chem. Lett. **8**, 2780 (2017).

[39] K. Fehre, N. M. Novikovskiy, S. Grundmann, G. Kastirke, S. Eckart, F. Trinter, J. Rist, A. Hartung, D. Trabert, C. Janke, *et al.*, Fourfold differential photoelectron circular dichroism, Phys. Rev. Lett. **127**, 103201 (2021).